Experimental realization of two-dimensional artificial skyrmion crystals at room temperature

B. F. Miao,[1] L. Sun,[1] Y. W. Wu,[1] X. D. Tao,[1] X. Xiong,[1] Y. Wen,[1] R. X. Cao,[1] P. Wang,[1] D. Wu,[1] Q. F. Zhan,[2] B. You,[1] J. Du,[1] R. W. Li,[2] and H. F. Ding[1,*]

[1]*National Laboratory of Solid State Microstructures and Department of Physics, Nanjing University, Collaborative Innovation Center of Advanced Microstructures, 22 Hankou Road, Nanjing 210093, People's Republic of China*

[2]*Key Laboratory of Magnetic Materials and Devices, Ningbo Institute of Materials Technology and Engineering, Chinese Academy of Sciences, Ningbo 315201, People's Republic of China*

(Received 8 April 2014; revised manuscript received 17 October 2014; published 11 November 2014)

We report the creation of an artificial skyrmion crystal, which is configurable reliably at *room temperature*. The samples are fabricated by embedding lithography-patterned arrays of micron-sized Co disks onto Co/Pt multilayer films that have perpendicular magnetic anisotropy. Kerr microscopy and magnetic force microscopy reveal that the disks are in the vortex state with controllable circulation. Via comparison of measured hysteresis loops and calculated ones, we find that the sample can be configured into either a skyrmion or a non-skyrmion state. The reproducible and stable skyrmion crystal at room temperature opens the door to direct exploration of their unique topological properties, which has deservedly caused a flurry of theoretical activity.

DOI: 10.1103/PhysRevB.90.174411 PACS number(s): 75.75.−c, 75.60.−d, 75.78.Cd, 78.20.Ls

I. INTRODUCTION

Magnetic skyrmion crystals have attracted great interest both theoretically and experimentally due to their unique physical properties and potential applications [1–16]. They are anticipated to produce unconventional spin-electronic phenomena, such as the topological Hall effect [1–4] and to exhibit novel dynamic properties [5–7]. The skyrmion crystal may be exploited as a new class of spintronic materials as it can be driven by a charge or spin current of ultralow density [8,9]. The skyrmion crystal also attracts interdisciplinary interest as an analog of similar lattice structures in nuclear physics [17,18], quantum Hall systems [19,20], and liquid crystals [21]. Experimentally, neutron scattering studies confirmed the existence of the skyrmion crystal within a narrow temperature/magnetic field region of particular three-dimensional (3D) helical magnets [10,11]. It was found that the two-dimensional (2D) skyrmion crystal can exist in a wider temperature/field range in comparison with 3D lattices [4,12]. However, the rarity and the narrow temperature-field region of the existence of the skyrmion crystal still impede its physical exploration. In particular, no skyrmion crystal has yet been reported to exist at room temperature. In addition, a skyrmion crystal typically arises from helical spin structures induced by the Dzyaloshinskii-Moriya (DM) interaction [22,23]. The DM interaction, however, is commonly weak, limiting the pool of prospective materials for the design of skyrmion crystals. To overcome these obstacles, alternative approaches to assemble skyrmion crystals have been proposed [24,25], such that the presence of DM interaction is not necessary, while at the same time these crystals could, in principle, be stabilized over wide temperature/field ranges. Despite this rapid theoretical development, to realize actual skyrmion crystals has remained an experimental challenge. In addition, questions about room-temperature stability and how to tailor their topological properties also need to be addressed.

A skyrmion can be viewed as a vortex in the center surrounded by out-of-plane magnetization that is oppositely aligned with the vortex core [12,26]. The spins continuously deform from up (down) in the center to down (up) along the periphery in all radial directions away from the center. Thus spins within one unit cell point in all directions wrapping a sphere. In order to form a 2D skyrmion crystal, all vortices need to bear the same circulation and their polarity should be aligned oppositely with the surrounding magnetization [see Fig. 1(a)]. To achieve this, micron- or submicron-size major-segment disk arrays are implanted into films with perpendicular magnetization [24]. Applying a field pulse along the cutting edge of the major-segment disk can align the vortex circulation [27–29]. Typically, the vertical switching fields for the vortex core and the perpendicular film are different, enabling the control of their relative orientation.

In this work we report the creation of an artificial skyrmion crystal, which is reproducible and configurable at *room temperature*. The samples are prepared by embedding lithography-patterned arrays of micron-size Co disks onto Co/Pt multilayer films that possess perpendicular magnetic anisotropy. Kerr microscopy imaging and magnetic force microscopy (MFM) demonstrate that the Co disks are in the vortex state where the circulation can be tuned. The measured hysteresis loops are quite similar to those obtained via micromagnetic simulations, revealing the sample can be configured into either skyrmion (skyrmion number $S = \pm 1$) or non-skyrmion ($S = 0$) states. As all the measurements are performed at room temperature, we demonstrate that skyrmion crystals can be stabilized at room temperature. The demonstration of actual skyrmion crystals at room temperature provides an interesting playground to further explore their unique properties.

II. SAMPLE FABRICATION PROCESS

We first deposit $[\mathrm{Pt}(0.5\,\mathrm{nm})/\mathrm{Co}(0.5\,\mathrm{nm})]_5/\mathrm{Pt}(5\,\mathrm{nm})$ on a Si(001) substrate by dc magnetron sputtering, where the 5-nm Pt film acts as a buffer layer. The hysteresis loop confirms that the film has perpendicular anisotropy, and the switching field

*Corresponding author: hfding@nju.edu.cn

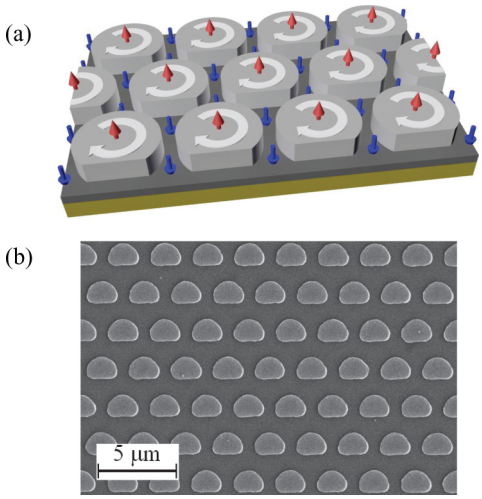

FIG. 1. (Color online) (a) Schematic of 2D artificial skyrmion crystal. Ordered arrays of magnetic disks are prepared on top of a film with perpendicular anisotropy. The arrows represent the magnetization orientation of the local moments. (b) Typical scanning electron microscopy image of the fabricated structure: disk diameter, 2 μm; lattice constant, 2.7 μm. The major-segment disk is made of 32-nm-thick Co, while the perpendicular anisotropy material beneath is a Co/Pt multilayer.

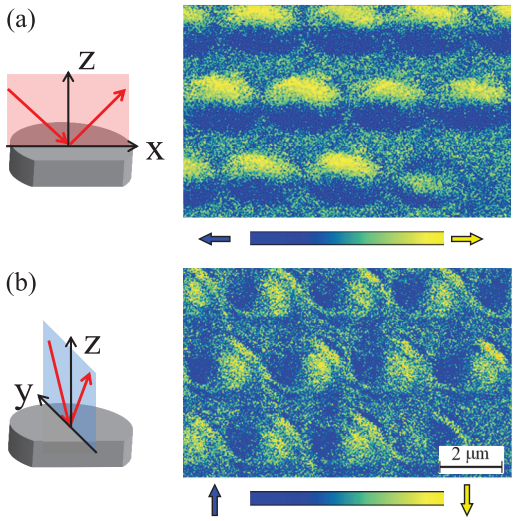

FIG. 2. (Color online) Kerr microscopy images with the sensitivities along the x axis (a) and the y axis (b). Blue (yellow) arrow denotes the magnetization component along the left (right) in (a), and up (down) in (b), respectively. Both images are obtained with longitudinal magneto-optical Kerr effect geometry with the corresponding schematic setups shown on the left. [Note that the weak stripe contrast found near the disk edges in (b) was caused by the imperfect background subtraction process.]

is ~1.3 kOe. After that, the sample is transferred for patterning by means of an ultraviolet lithography system. A Co film of 32 nm is then deposited by electron beam evaporation onto the prepatterned sample. After lift-off, edge-clipped circular disk arrays with the diameter ~2 μm and a cutting angle of ~90° are obtained [see Fig. 1(b)]. The center-to-center separation between neighboring Co disks is ~2.7 μm. As will be demonstrated below, the Co disk in this major-segment geometry has a vortex ground state and its circulation can be controlled by in-plane magnetic field pulses.

III. RESULTS AND DISCUSSION

A vortex has four degenerate states with clockwise (CW) or counterclockwise (CCW) circulation, and up or down polarity. We perform the following manipulation sequence in order to format all Co disks into uniform polarity and circulation. First, a weak in-plane magnetic field (0.2 kOe) along the disk clipped edge is applied to saturate the Co disks into a single domain. After releasing it, most of the disks would deform into vortices with the same circulation. Second, a perpendicular field of 10 kOe (which is slightly smaller than the saturation field 13 kOe) is applied to format the vortex cores and surrounding material into a parallel configuration. Upon turning off this field, the disks remain in a vortex state with all the core magnetization pointing to the field direction. At last, a smaller perpendicular field of −1.5 kOe is applied to align the disk periphery antiparallel with the vortex cores. In such a case, the vortex-core polarities remain unchanged and they are antiparallel with the surrounding Co/Pt multilayers. Thus, a skyrmion lattice is stabilized.

To confirm that the disks are in the vortex state, we first performed Kerr microscopy measurements. Figures 2(a) and 2(b) present the Kerr images in two longitudinal geometries. In these geometries, the contrast represents the in-plane magnetization along the optical plane. As shown in the sketches in Fig. 2, the optical planes in these two geometries are aligned perpendicular to each other, i.e., along or perpendicular to the cutting edge direction. In such a case, the Kerr signal is sensitive to the magnetization along/perpendicular to the clipped edge in Figs. 2(a) and 2(b), respectively. In order to remove the morphology contrast and the residual polar Kerr contributions, we used a background subtraction technique. We found the disks can be saturated into a uniform single domain state upon applying an in-plane field of 0.2 kOe. The averaged image obtained with ±0.2 kOe is chosen as the background. Figure 2(a) depicts the magnetization component along the clipped edge in zero field after the background subtraction. The Co disks have a contrast between up and down portions, reflecting an opposite magnetization component along the x direction. Remarkably, most of the disks, except the one at the bottom right, show bright contrast on top and dark contrast at the bottom, suggesting they are mostly in the same magnetic configurations. The contrast suggests the disks can be either in two-domain or vortex states. In order to identify the magnetic configuration of the Co disks, we rotated the optical plane by 90° and performed the same measurements. If the disks are in vortex states, the contrast should also rotate 90° accordingly [30]. Because the domain wall typically has a width on the order of tens of nanometers, which makes it unresolved within the limitations of Kerr microscopy, there will be no contrast for the two-domain configuration. Figure 2(b) shows the result of the same spot after rotating the optical plane by 90°. The image has contrast between left and right portions, i.e., the contrast rotates following the rotation of the

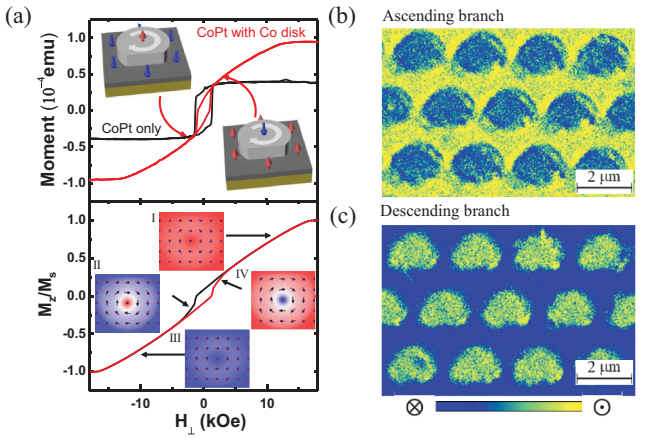

FIG. 3. (Color online) (a) Upper panel: Hysteresis loops along the vertical direction for $[Pt(0.5\,nm)/Co(0.5\,nm)]_5/Pt(5\,nm)/Si$ substrate with (red) and without (black) Co disks. The insets show two skyrmions under different magnetic fields. The arrows represent the magnetization orientation of the local moments. Lower panel: The calculated hysteresis loop obtained using parameters defined in the text. The insets show the top view of magnetic configuration of the Co/Pt layer in a calculated artificial skyrmion crystal at different stages. In order to clearly show the contrast of the vortex core and surrounding material, the Co-disk diameter is set as 120 nm with a 150-nm separation. Polar Kerr microscopy images under perpendicular field: (b) and (c) present the magnetic contrast along the ascending branch and descending branch, respectively. Cross (dot) in a circle denotes the magnetization component pointing into (out of) the plane, respectively. The seemingly visual difference between the disks in (b) and (c) is only caused by the different (bright/dark) surrounding background.

optical plane. This unambiguously proves that the disks are in the vortex state. From their contrasts, we can identify that 12 of 13 disks shown in the image have the same CW circulation. We note that the weak contrast near the disk edge in Fig. 2(b) originates from the imperfect background subtraction.

The upper panel of Fig. 3(a) presents a hysteresis loop measured by a superconducting quantum interference device (SQUID) for Co/Pt multilayers (black curve, with a dimension $\sim$2.5 mm $\times$ 3.5 mm), which exhibits a sizable perpendicular anisotropy with a coercivity of $\sim$1.3 kOe. For comparison, we also plot the hysteresis loop after the Co-disk deposition in the same figure. After coating the Co disks, the switching field of the film is sizably reduced to $\sim$0.9 kOe. The reduced coercivity demonstrates that there is ferromagnetic coupling between the Co disks and the underneath Co/Pt multilayer as the in-plane magnetization of Co disk acting as an effective transverse field which softens the Co/Pt multilayer. Meanwhile, the switching amplitude is also reduced to 60% of the value that prior to the Co-disk deposition, is in good agreement with the estimated area ratio (55%). The reduced amplitude in the jump evidences that the Co/Pt multilayers underneath the Co disks are no longer perpendicular due to the strong coupling between them. This is consistent with the previous calculation [24] and the following micromagnetic simulations that the vortex state penetrates into the Co/Pt multilayers underneath the disks. In addition, the polar Kerr microscopy measurements are also performed to depict the out-of-plane magnetization

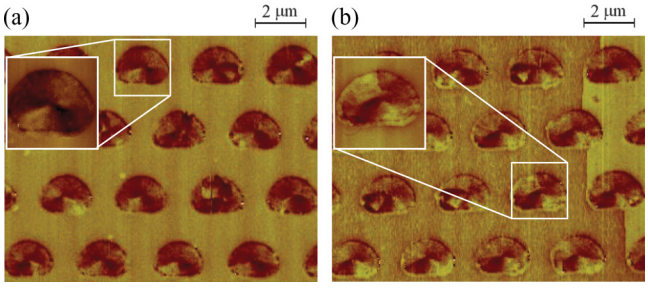

FIG. 4. (Color online) MFM image of two skyrmion states. The alternating dark and bright contrasts indicate the Co disks are in vortex state. The insets of (a) and (b) present the zoomed-in image of a single vortex. A small portion of the underlying CoPt multilayer in the right edge did not switch, and thus, acted as a reference point.

component. The magnetic contrast along the ascending branch is obtained by subtracting the image at $\sim$1.0 kOe (switched) by that at $\sim$0.9 kOe (preswitched) [Fig. 3(b)]. Similarly, one can obtain the image for the descending branch of the hysteresis loop [Fig. 3(c)]. The surrounding CoPt film changes from bright to dark reflecting the switching of the magnetization direction. The sharp contrast between Figs. 3(b) and 3(c) demonstrates that the surrounding Co/Pt multilayer can be controlled by a perpendicular magnetic field.

To further confirm our findings, we also performed the MFM measurements. For a perfect circular vortex disk, the MFM image typically exhibits a dark or bright spot at the disk center only [31]. For a nonperfect disk such as an elliptical one, the vortex is no longer perfectly circular and the stray field also exists in the surrounding part. In such case, a pattern of four quadrants with alternating dark and bright contrasts is expected [32,33]. Figure 4(a) shows the typical MFM image of our patterned structure. Except several disks which have fine structures (may possess a multivortex/multidomain state [34]), most of the disks (23 out of 28 disks examined) clearly show four quadrants with alternating dark and bright contrasts evidencing that they are in the vortex state since the edge-clipped circular disk naturally has a shape asymmetry. Two kinds of patterns of four quadrants in the disks correspond to CW or CCW circulation, respectively. From the patterns, we find that most of the vortices have the same circulation, which is consistent with the Kerr microscopy images in Fig. 2. Figure 4(b) presents the MFM image with opposite vortex circulation with respect to Fig. 4(a) after the field operation. We purposely chose an opposite perpendicular field close to the switching field of surrounding CoPt multilayers, $\sim$0.9 kOe. Thus, one can notice a small portion of the CoPt film in the right side did not switch and shows opposite magnetization with respect to the left part.

To better understand the physical origin of the hysteresis loops, we also performed micromagnetic simulations using the OOMMF code [35]. The material parameters are the same as those we used previously [24] except for the magnetization and perpendicular anisotropy constant of the Co/Pt multilayer. For these two values, we took our experimentally measured data: 8.7×10^5 J/m and 532 J/m^3, respectively. To accommodate the large sample size, the cell size is also enlarged to

$20 \times 20 \times 1\,\text{nm}^3$ for the hysteresis calculations. We also cross-checked some calculations with the cell size of $5 \times 5 \times 1\,\text{nm}^3$ at certain fields (zero field, prior and after the switching of the perpendicular film and the vortex core) and found the results are essentially the same. The lower panel of Fig. 3(a) presents the calculated hysteresis loop with insets that show a sketch of the magnetic configurations at the corresponding fields. The red (black) curve shows ascending (descending) branches of the hysteresis, respectively. In the insets, the red/blue color denotes the out-of-plane magnetization, while the gray arrow represents the vortex circulation. The sample is fully saturated at 16 kOe; the vortex state then evolves with decreasing field. Both the vortex cores and the surrounding Co/Pt multilayers are aligned with the field direction, as shown in inserts I and III in the lower panel of Fig. 3(a). For a vortex or antivortex, the skyrmion number is defined as half of the product of the winding number and the polarity. The winding number equals $1/-1$ for a vortex/antivortex, respectively, independent of their CW or CCW circulation [36]. Therefore, the two states mentioned above (insets I and III) have skyrmion number $S = 0$ since the unit cell can be considered to be a combination of a vortex and an antivortex bearing the same polarity. After reversing the field, the hysteresis involves two-step switching at a field of $\sim$1.3 kOe and $\sim$5.0 kOe, corresponding to the switching of the surrounding Co/Pt films and the vortex cores, respectively. This is not surprising since it was reported experimentally that a submicron Py disk switches its core at $\sim$3 kOe [33]. The vortex-core switching energy barrier was estimated to roughly scale linearly with the nearest neighbor interaction [37]. Thus, one can estimate the switching field for the Co vortex core to be $\sim$5.7 kOe in good agreement with our calculation, $\sim$5.0 kOe. The second switching is small and more clearly visible with the amplified view. This can be understood since the vortex core is only $\sim$40 nm in diameter at zero field and becomes even smaller before its switching [24]. In comparison with the several-micron-size unit cell area, it is almost negligible. To further identify this, we also performed simulations for 90-nm-diameter disk arrays with a separation of 120 nm implanted onto the Co/Pt layer. With these conditions, the second jump becomes more pronounced, confirming the above analysis. Since the vortex cores and the surrounding Co/Pt film have different switching fields, they can be aligned into an antiparallel configuration, giving rise to the skyrmion state as shown in insets II and IV of the lower panel in Fig. 3(a). We note the skyrmion numbers of insets II and IV are 1 and -1, respectively, due to their opposite magnetization in the vertical component. They also have opposite sign for the effective DM interaction constant. In short, the sample goes through states with skyrmion numbers $S = 0, -1, 0, +1$ within one hysteresis loop, demonstrating the configurability of the different states. Interestingly, we find that all four states shown in the insets in the lower panel of Fig. 3(a) can be stabilized at zero field. The simulated hysteresis loop is similar to the measured one, except the vortex-core switching was not resolved experimentally due to the limited sensitivity. The difference in the switching fields for the vortex core and the surrounding Co/Pt film, however, still enables the control of the skyrmion states. During the switching between each state, we found the transitions are accompanied with spin wave excitations, which is consistent with the change of topological (skyrmion) number [26]. Figure 5 exhibits the in-plane component magnetization along the x axis, while the red/blue color denotes the magnetization pointing to right/left, respectively. One can find spin wave excitations, as highlighted in the black ellipses, reflecting that the transition between different topological states is not smooth. Similar effects have been discussed in the reversal process of the vortex and antivortex cores [26,38,39].

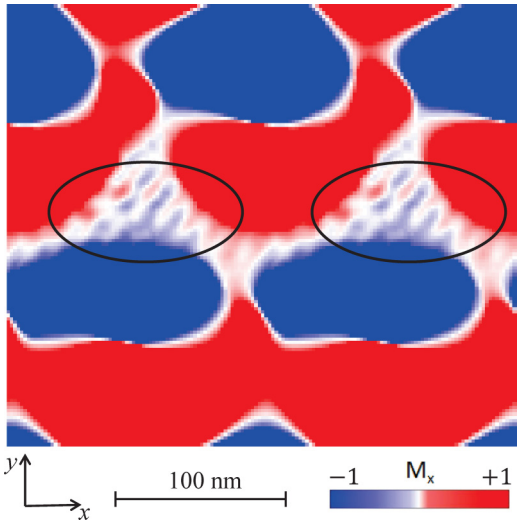

FIG. 5. (Color online) Top view of magnetic configuration during the transition from a non-skyrmion state to a skyrmion state. The spin waves are spotted in the black ellipses. In the calculation, we use material parameters defined in the paper. The diameter and lattice constant are 120 and 150 nm, respectively. The red/blue colors indicate local moments pointing to the right/left, respectively. To better visualize the spin waves, the contrast was significantly enhanced.

We point out that our findings, at first glimpse, might appear similar to the previous observation of vortices and vortex arrays [31,40–42]. However, they are topologically different. A vortex has its magnetization direction pointing to half of a sphere only, thus yielding a skyrmion number $\pm 1/2$ [36]. In our case, the vortex is fully surrounded by a perpendicular magnetization with the direction oppositely aligned with respect to the vortex-core magnetization. This unique configuration makes the magnetization point to all the directions wrapping a sphere and yields a skyrmion number of $S = \pm 1$ per unit cell. In such case, a skyrmion crystal is created. Here we demonstrated that this kind of skyrmion crystal can be stabilized at room temperature.

IV. SUMMARY

In summary, we have created an artificial skyrmion crystal which is reproducible, reliable, and configurable at *room temperature*. Kerr microscopy images along two orthogonal directions and magnetic force microscopy measurements identify that the Co disks embedded on the perpendicular Co/Pt multilayers are in the vortex state with controllable circulation. By comparing the measured hysteresis loop and the micromagnetic simulations, we show that the sample can be readily configured into states with skyrmion numbers -1,

0, and +1. The creation of a functional skyrmion crystal at room temperature opens the door to the exploration of unique fundamental properties such as the room-temperature topological Hall effect or exotic spin dynamics. The reported advance casts the potential for the production of high-density storage devices, based on fully controllable skyrmion-lattice arrays at room temperature and higher.

Note added. Recently, we became aware of the observation of a single artificial skyrmion by Li *et al.*, using photoemission electron microscopy [43]. In this work, we report the observation of an artificial skyrmion lattice with controllable skyrmion number.

ACKNOWLEDGMENTS

This work is supported by the National Basic Research Program of China (Grant No. 2010CB923401, and No. 2011CB922103), the National Natural Science Foundation of China (Grants No. 11374145, No. 11304150, and No. 11023002), and the Natural Science Foundation of Jiangsu (Grant No. BK2012300). We thank Dr. L. Chen for the help with Kerr microscopy measurements and Professor S. L. Tang for the help with magnetic force microscopy measurements. Critical reading of the manuscript by Dr. S. D. Bader is gratefully acknowledged.

[1] Y. Onose, N. Takeshita, C. Terakura, H. Takagi, and Y. Tokura, Phys. Rev. B **72**, 224431 (2005).

[2] A. Neubauer, C. Pfleiderer, B. Binz, A. Rosch, R. Ritz, P. G. Niklowitz, and P. Böni, Phys. Rev. Lett. **102**, 186602 (2009).

[3] M. Lee, W. Kang, Y. Onose, Y. Tokura, and N. P. Ong, Phys. Rev. Lett. **102**, 186601 (2009).

[4] S. X. Huang and C. L. Chien, Phys. Rev. Lett. **108**, 267201 (2012).

[5] O. Petrova and O. Tchernyshyov, Phys. Rev. B **84**, 214433 (2011).

[6] M. Mochizuki, Phys. Rev. Lett. **108**, 017601 (2012).

[7] Y. Onose, Y. Okamura, S. Seki, S. Ishiwata, and Y. Tokura, Phys. Rev. Lett. **109**, 037603 (2012).

[8] X. Z. Yu, N. Kanazawa, W. Z. Zhang, T. Nagai, T. Hara, K. Kimoto, Y. Matsui, Y. Onose, and Y. Tokura, Nat. Commun. **3**, 988 (2012).

[9] F. Jonietz, S. Mühlbauer, C. Pfleiderer, A. Neubauer, W. Münzer, A. Bauer, T. Adams, R. Georgii, P. Böni, R. A. Duine, K. Everschor, M. Garst, and A. Rosch, Science **330**, 1648 (2010).

[10] S. Mühlbauer, B. Binz, F. Jonietz, C. Pfleiderer, A. Rosch, A. Neubauer, R. Georgii, and P. Böni, Science **323**, 915 (2009).

[11] W. Münzer, A. Neubauer, T. Adams, S. Mühlbauer, C. Franz, F. Jonietz, R. Georgii, P. Böni, B. Pedersen, M. Schmidt, A. Rosch, and C. Pfleiderer, Phys. Rev. B **81**, 041203 (2010).

[12] X. Z. Yu, Y. Onose, N. Kanazawa, J. H. Park, J. H. Han, Y. Matsui, N. Nagaosa, and Y. Tokura, Nature (London) **465**, 901 (2010).

[13] X. Z. Yu, N. Kanazawa, Y. Onose, K. Kimoto, W. Z. Zhang, S. Ishiwata, Y. Matsui, and Y. Tokura, Nat. Mater. **10**, 106 (2011).

[14] A. Fert, V. Cros, and J. Sampaio, Nat. Nanotechnol. **8**, 152 (2013).

[15] J. Sampaio, V. Cros, S. Rohart, A. Thiaville, and A. Fert, Nat. Nanotechnol. **8**, 839 (2013).

[16] N. Nagaosa and Y. Tokura, Nat. Nanotechnol. **8**, 899 (2013).

[17] T. H. R. Skyrme, Nucl. Phys. **31**, 556 (1962).

[18] I. Klebanov, Nucl. Phys. B **262**, 133 (1985).

[19] S. L. Sondhi, A. Karlhede, S. A. Kivelson, and E. H. Rezayi, Phys. Rev. B **47**, 16419 (1993).

[20] L. Brey, H. A. Fertig, R. Côté, and A. H. MacDonald, Phys. Rev. Lett. **75**, 2562 (1995).

[21] A. N. Bogdanov, U. K. Rößler, and A. A. Shestakov, Phys. Rev. E **67**, 016602 (2003).

[22] I. Dzyaloshinsky, J. Phys. Chem. Solids **4**, 241 (1958).

[23] T. Moriya, Phys. Rev. **120**, 91 (1960).

[24] L. Sun, R. X. Cao, B. F. Miao, Z. Feng, B. You, D. Wu, W. Zhang, A. Hu, and H. F. Ding, Phys. Rev. Lett. **110**, 167201 (2013).

[25] Y. Y. Dai, H. Wang, P. Tao, T. Yang, W. J. Ren, and Z. D. Zhang, Phys. Rev. B **88**, 054403 (2013).

[26] O. A. Tretiakov and O. Tchernyshyov, Phys. Rev. B **75**, 012408 (2007).

[27] R. K. Dumas, T. Gredig, C.-P. Li, I. K. Schuller, and K. Liu, Phys. Rev. B **80**, 014416 (2009).

[28] M. Schneider, H. Hoffmann, and J. Zweck, Appl. Phys. Lett. **79**, 3113 (2001).

[29] K.-M. Wu, L. Horng, J.-F. Wang, J.-C. Wu, Y.-H. Wu, and C.-M. Lee, Appl. Phys. Lett. **92**, 262507 (2008).

[30] H. F. Ding, A. K. Schmid, D. Li, K. Y. Guslienko, and S. D. Bader, Phys. Rev. Lett. **94**, 157202 (2005).

[31] T. Shinjo, T. Okuno, R. Hassdorf, K. Shigeto, and T. Ono, Science **289**, 930 (2000).

[32] A. Hubert and R. Schaefer, *Magnetic Domains* (Springer, Berlin, 1998).

[33] T. Okuno, K. Shigeto, T. Ono, K. Mibu, and T. Shinjo, J. Magn. Magn. Mater. **240**, 1 (2002).

[34] I. L. Prejbeanu, M. Natali, L. D. Buda, U. Ebels, A. Lebib, Y. Chen, and K. Ounadjela, J. Appl. Phys. **91**, 7343 (2002).

[35] M. J. Donahue and D. G. Porter, OOMMF User's Guide Version 1.0, National Institute of Standards and Technology, Gaithersburg, MD, 1999.

[36] C. L. Chien, F. Q. Zhu, and J.-G. Zhu, Phys. Today **60**(6), 40 (2007).

[37] A. Thiaville, J. M. García, R. Dittrich, J. Miltat, and T. Schrefl, Phys. Rev. B **67**, 094410 (2003).

[38] B. Van Waeyenberge, A. Puzic, H. Stoll, K. W. Chou, T. Tyliszczak, R. Hertel, M. Fahnle, H. Bruckl, K. Rott, G. Reiss, I. Neudecker, D. Weiss, C. H. Back, and G. Schutz, Nature (London) **444**, 461 (2006).

[39] R. Hertel, S. Gliga, M. Fähnle, and C. M. Schneider, Phys. Rev. Lett. **98**, 117201 (2007).

[40] H. Shima, V. Novosad, Y. Otani, K. Fukamichi, N. Kikuchi, O. Kitakamai, and Y. Shimada, J. Appl. Phys. **92**, 1473 (2002).

[41] A. Vogel, A. Drews, T. Kamionka, M. Bolte, and G. Meier, Phys. Rev. Lett. **105**, 037201 (2010).

[42] M.-Y. Im, P. Fischer, K. Yamada, T. Sato, S. Kasai, Y. Nakatani, and T. Ono, Nat. Commun. **3**, 983 (2012).

[43] J. Li, A. Tan, K. W. Moon, A. Doran, M. A. Marcus, A. T. Young, E. Arenholz, S. Ma, R. F. Yang, C. Hwang, and Z. Q. Qiu, Nat. Commun. **5**, 4704 (2014).